Research Article Vol. 37, No. 7 / July 2020 / Journal of the Optical Society of America A 1155

Journal of the Optical Society of America A

OPTICS, IMAGE SCIENCE, AND VISION

Superconical aplanatic ovoid singlet lenses

ALBERTO SILVA-LORA AND RAFAEL TORRES*

Grupo de Óptica y Tratamiento de Señales, Universidad Industrial de Santander, Bucaramanga, Colombia
**Corresponding author: rafael.torres@saber.uis.edu.co*

Received 16 March 2020; revised 29 May 2020; accepted 2 June 2020; posted 2 June 2020 (Doc. ID 392795); published 25 June 2020

In this work, we return to Descartes's idea to develop a formalism to construct rigorously stigmatic singlet lenses comprising two Cartesian surfaces. Optical systems are built using a considerable number of spherical surfaces, presenting in most cases spherical aberration. Wasermann and Wolf proposed eliminating spherical aberration and minimizing third-order coma by using two adjacent aspherical surfaces. That is why, using a parametric formulation for Cartesian ovals, we propose the design of singlet lenses where the condition of rigorous stigmatism is guaranteed for each surface, and therefore, strictly speaking, in the pair of stigmatic points, the lens becomes an optical system free of spherical aberration. This formulation is unified to both refractive and reflective optical surfaces. Therefore, within the framework of the theory of rigorously stigmatic optical systems, making use of Cartesian surfaces for the construction of stigmatic ovoid singlet lenses, we achieve the same functionality of optical systems involving a set of spherical lenses. These lenses have the advantage of being formulated according to a generalized shape factor associated with the Coddington shape factor, allowing an easy classification of these stigmatic lenses. The ideal imaging is carried out by applying an exact ray-tracing method through these ovoid singlet lenses.

https://doi.org/10.1364/JOSAA.392795

1. INTRODUCTION

Spherical surfaces prevail in the design of optical devices [1], and these generally introduce spherical aberration in imaging systems, but a set of spherical surfaces, in the appropriate configuration, allows minimizing this type of aberration. Additionally, the aspherical surfaces [1] can also minimize or eliminate spherical aberration by using one or two of them. Aspherical surfaces are all those surfaces that are not spherical, including the rigorously stigmatic or Cartesian surfaces [2–5], that differ from other aspherical surfaces in that they are the only rigorously stigmatic optical surfaces. These surfaces were deduced by Descartes [6] and then studied by Huygens [7], who introduces the problem for the design of spherical aberration-free singlet lenses using two aspherical surfaces. Aspherical surfaces play an essential role in the area of optical design so that, through their use, it is possible to reduce the number of surfaces of the optical system to obtain good-quality imaging systems [8]. As technology advances, optical devices are required to be smaller, maintaining excellent quality. In order to achieve these requirements, aspherical surfaces are implemented impetuously in several works for the design of microlenses [9–12], used in imaging systems for mobile devices. These types of surfaces are also implemented in the design of compound refractive lens (CRL) systems [13], lighting systems [14], and the design of biparabolic singlet lenses [15] and immersion lenses [16].

Huygens's work is related to the problem of spherical aberration-free image formation for a couple of conjugate points, but it was Herschel [17] who added a new condition, which states that the system may be free from spherical aberration for its conjugated points and two neighboring conjugated points. It was not until Abbe's publication [18] that the term aplanatism was related to the extension of stigmatism for off-axis points. Aplanatism is another essential property for the design of imaging systems, e.g., systems composed by two reflective optical surfaces [19,20], or by a combination of a refractive and a reflective optical surface [21,22]. The problem of obtaining an aplanatic system was formulated by Wassermann and Wolf [23–25], who proposed the introduction of the aspherical surfaces as a corrective that allows an optical imaging system to be simultaneously free of spherical and coma aberration [26]. This solution has been addressed both analytically [27] and numerically [28]. Some authors have partially solved the problem [29–32] by defining a first surface that induces aberrations and finding a second one that compensates for them. Another approach to obtain singlet lenses free of spherical aberration is to consider using two Cartesian surfaces [33].

In this work, we address the problem by designing singlet lenses free of spherical aberration using Cartesian or rigorously stigmatic surfaces [7] as is shown in Ref. [33]. From a parametric formulation for Cartesian surfaces using polar parameters [34], formulated by our group, we have adapted a new formulation as a generalization of the Schwarzschild expression for conics [35],

by taking advantage of the implicit form of Cartesian surfaces as a particular case of superconic surfaces [36]. This formulation differs from [33] in that this one includes both refractive and reflective cases, including all degenerated cases (conic surfaces), and sign conventions are not necessary. The formulation proposed here is linked to a generalized Coddington shape factor, allowing the design of lenses with different shapes capable to produce a perfect imaging of a point object located on the optical axis. We will refer to this type of singlet lenses as *stigmatic ovoid singlet lenses* (SOSL). Additionally, an exact ray tracing is carried out using the vector Snell–Descartes law, corroborating the perfect imaging of a point object on the optical axis. Using this method is also shown the performance of these lenses to image an off-axis point object considering different values of the shape factor.

2. EXPLICIT EXPRESSION FOR CARTESIAN OVALS

A Cartesian refracting surface [6,37] is a surface that can form stigmatic point image from a point object. Figure 1 shows cross sections of a Cartesian oval in a longitudinal and transversal plane, where A and A' are its stigmatic points, and all rays are traveling the same optical path length (OPL). Assuming a Cartesian coordinates system, the vector quantities are defined as $\vec{\rho}=(x,y,z)$ and $\vec{r}=(x,y)$, where x and y are transversal coordinates and z is the longitudinal coordinate. The surface Σ is such that it can form a perfect point image at a distance $z_i=\overline{\mathcal{O}A'}$ from a point object at a distance $z_o=\overline{\mathcal{O}A}$. Explicit and parametric formulation of these surfaces are of great interest in the design and manufacture of new optical devices [4,13,32,38].

Considering $\rho=\sqrt{x^2+y^2+z^2}$ as the distance between the origin of the coordinates system and a point on the Cartesian surface, it is shown in Ref. [34] that this condition, under Fermat's sign rule, allows us to obtain an implicit expression for Cartesian surfaces as a function of variables ρ and z, written as

$$\begin{aligned}&[(n_i^2-n_o^2)\rho^2-2z(n_i^2z_i-n_o^2z_o)]^2\\&-4n_in_o(n_iz_i-n_oz_o)(n_oz_i-n_iz_o)\rho^2\\&-8n_in_oz_iz_o(n_iz_i-n_oz_o)(n_i-n_o)z=0.\end{aligned}\tag{1}$$

This formula has the advantage of being valid for both refractive and reflective surfaces. The reflective ones are obtained by replacing $n_i=-n_o$, but this condition should not be confused with metamaterials.

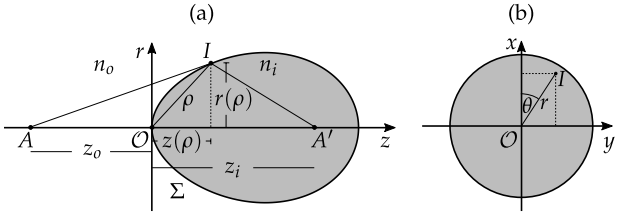

Fig. 1. Graphical representation of Cartesian surfaces. (a) Longitudinal and (b) transversal cross section of a Cartesian oval.

Both explicit and parametric formulations are usual, but the explicit and parametric ones are easier to manipulate and determine edge thickness. That is why explicit and parametric expressions for Cartesian surfaces could be of great interest in the optical design area. Some explicit [4,5,13] and parametric [34,39] expressions for Cartesian surfaces have been developed, but none of these expressions is available in lens design software as a standard formulation [40]. According to [34,39], Cartesian surfaces can also be expressed implicitly as a degenerated form of a family of surfaces known as superconic [36], written as

$$\begin{aligned}&c_0Gz^2-2(1+b_1\rho^2+b_2\rho^4+\cdots)z\\&+(c_0+c_1\rho^2+c_2\rho^4+\cdots)\rho^2=0,\end{aligned}\tag{2}$$

where the parameters G and c_0, along with parameters c_i and b_i with $i=1,2,\ldots$, are known as form parameters. Equation (1) can be expressed as a particular case of superconic surfaces by dividing it by $4n_in_oz_iz_o(n_i-n_o)(n_iz_i-n_oz_o)$. We define four form parameters $(GOTS)$ as follows:

$$G=\frac{(n_i^2z_i-n_o^2z_o)^2}{n_in_o(n_iz_i-n_oz_o)(n_iz_o-n_oz_i)},\tag{3}$$

$$O=\frac{n_iz_o-n_oz_i}{z_iz_o(n_i-n_o)},\tag{4}$$

$$T=\frac{(n_i-n_o)(n_i+n_o)^2}{4n_in_oz_iz_o(n_iz_i-n_oz_o)},\tag{5}$$

$$S=\frac{(n_i+n_o)(n_i^2z_i-n_o^2z_o)}{2n_in_oz_iz_o(n_iz_i-n_oz_o)},\tag{6}$$

and using these parameters, Eq. (1) can be written as

$$f(x,y,z)=OGz^2-2(1+S\rho^2)z+(O+T\rho^2)\rho^2=0.\tag{7}$$

Thus, if parameters c_i and b_i (with $i=2,3,\ldots$) of Eq. (7) vanish, we can see that, taking $O=c_0$, $T=c_1$, and $S=b_1$, these superconic surfaces degenerate into Cartesian surfaces given by Eq. (7).

A. Parametric Expression for Cartesian Surfaces

Here we take the formulation of Cartesian surfaces as a particular case of superconic, to formulate a parametric expression. Hence, solving Eq. (7) as a quadratic equation in z, the exact expression for the sag $z(\rho)$ is obtained, given by

$$z=\frac{\left(1+S\rho^2\pm\sqrt{1+(2S-O^2G)\rho^2+(S^2-GOT)\rho^4}\right)}{OG}.\tag{8}$$

The solution that has optical significance is the one that goes through the origin of coordinates $\mathcal{O}$, so here is adopted the minus sign for which $z\to 0$, while $\rho\to 0$. From Eqs. (3)–(6) we can obtain the relation $S^2=GOT$, and then only three form parameters are independent. Using this relation in Eq. (8), we get rid of the quartic term in the radical. Rewriting Eq. (8), we obtain

$$z=\frac{1}{OG}\left(1+S\rho^2-\sqrt{1+(2S-O^2G)\rho^2}\right).\tag{9}$$

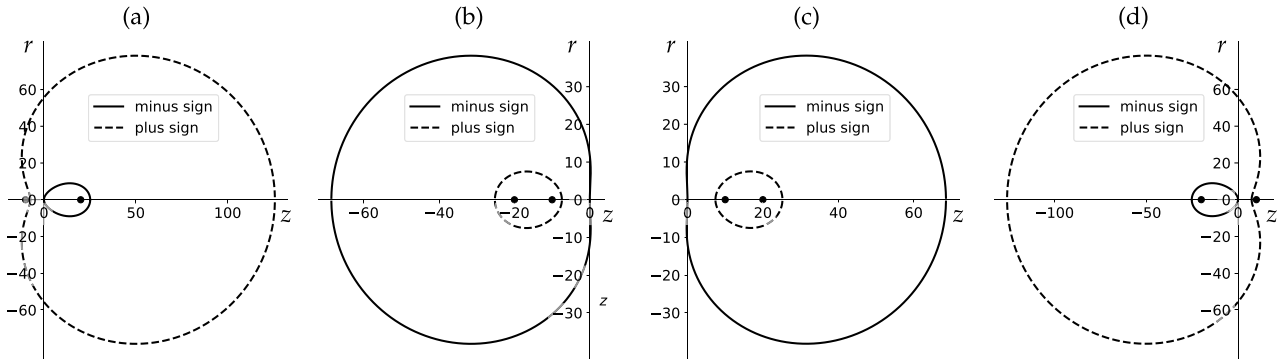

Fig. 2. Cartesian surfaces: the indices of refraction are maintained fixed, $n_o = 1$ and $n_i = 1.7$, while object and image position vary: (a) $z_o = -10$ and $z_i = 20$, (b) $z_o = -10$ and $z_i = -20$, (c) $z_o = 10$ and $z_i = 20$, (d) $z_o = 10$ and $z_i = -20$.

Rationalizing, we get

$$z(\rho) = \frac{(O + T\rho^2)\rho^2}{1 + S\rho^2 + \sqrt{1 + (2S - O^2G)\rho^2}}, \tag{10}$$

and using the relation (see Fig. 1)

$$r(\rho) = \pm\sqrt{\rho^2 - z^2(\rho)} \tag{11}$$

we obtain the transversal coordinate. Equations (10) and (11) are the parametric formulas of Cartesian surfaces, and they are the main result of this section for the design of lenses composed of these surfaces. In Fig. 2 are shown some examples of sections in the meridional plane, where the solid line represents the solution that passes through the origin of coordinates, and the dashed line is the solution obtained when the plus sign in Eq. (8) is considered, showing how these two solutions make a transition from the inner to the outer surface of the quartic and how these solutions consider both positive (surface opens right) and negative (surface opens left) surfaces.

B. Schwarzschild Equation as Particular Case

The degenerated cases are obtained by choosing the right values of the indices of refraction, the point object position, and the point image position, such that $T = S = 0$, reducing Eq. (10) to the expression

$$z(\rho) = \frac{O\rho^2}{1 + \sqrt{1 - O^2G\rho^2}}, \tag{12}$$

which can mathematically represent all the complete conic surfaces and can be written as a function of r by making the substitution $\rho^2 = z^2 + r^2$. After this substitution are obtained two solutions, where the one of optical interest is that passing through the origin of coordinates, written as follows:

$$z(r) = \frac{Or^2}{1 + \sqrt{1 - (K+1)O^2r^2}}, \tag{13}$$

where G reduces to the conic Schwarzschild constant K. The resulting Eq. (13) is known as the Schwarzschild equation [35] for conic surfaces. Equation (10) establishes a generalized Schwarzschild equation for Cartesian surfaces with $GOTS$ parameters. In Table 1 are shown all conic surfaces corresponding to the degenerated cases of Cartesian surfaces, both refracting and reflecting optical surfaces concerning the values of the indices of refraction, points object and point image positions.

Table 1. Degenerated Cases of Refractive and Reflective According to the Indices of Refraction, Object, and Image Position[a]

Surface	n_i	z_o	z_i	G	O	T	S
Ellipsoidal refractive	$n_i > n_o$	∞	z_i	$-(\frac{n_o}{n_i})^2$	$\frac{n_i}{z_i(n_i - n_o)}$	0	0
Hyperboloidal refractive	$n_i < n_o$	∞	z_i	$-(\frac{n_o}{n_i})^2$	$\frac{n_i}{z_i(n_i - n_o)}$	0	0
Hyperboloidal refractive	$n_i > n_o$	z_o	∞	$-(\frac{n_i}{n_o})^2$	$-\frac{n_o}{z_o(n_i - n_o)}$	0	0
Ellipsoidal refractive	$n_i < n_o$	z_o	∞	$-(\frac{n_i}{n_o})^2$	$-\frac{n_o}{z_o(n_i - n_o)}$	0	0
Spherical refractive	n_i	z_o	z_o	$\frac{(n_i + n_o)^2}{n_i n_o}$	$\frac{1}{z_o}$	$\frac{(n_i + n_o)^2}{4n_i n_o z_o^3}$	$\frac{(n_o + n_i)^2}{2n_i n_o z_o^2}$
Ellipsoidal reflective	$-n_o$	$z_o > 0$	$z_i > 0$	$-(\frac{z_i - z_o}{z_i + z_o})^2$	$\frac{z_i + z_o}{2z_i z_o}$	0	0
Ellipsoidal reflective	$-n_o$	$z_o < 0$	$z_i < 0$	$-(\frac{z_i - z_o}{z_i + z_o})^2$	$\frac{z_i + z_o}{2z_i z_o}$	0	0
Hyperboloidal reflective	$-n_o$	$z_o > 0$	$z_i < 0$	$-(\frac{z_i - z_o}{z_i + z_o})^2$	$\frac{z_i + z_o}{2z_i z_o}$	0	0
Hyperboloidal reflective	$-n_o$	$z_o < 0$	$z_i > 0$	$-(\frac{z_i - z_o}{z_i + z_o})^2$	$\frac{z_i + z_o}{2z_i z_o}$	0	0
Paraboloidal reflective	$-n_o$	∞	z_i	-1	$\frac{1}{2z_i}$	0	0
Paraboloidal reflective	$-n_o$	z_o	∞	-1	$\frac{1}{2z_o}$	0	0

[a]For each of the combinations between these parameters the values of the form parameters for conic surfaces of revolution are obtained.

The parameter O in Eq. (13) is the curvature, and an extrapolation leads us to define O as the curvature in the vertex of any Cartesian surface, also known as the axial curvature. In this way, we define O as the paraxial curvature of a Cartesian ovoid. We define G as the Cartesian ovoid constant, which is reduced to the conic or Schwarzschild constant for the degenerated cases of Cartesian surfaces. Using this formulation, in the following section we study how two Cartesian surfaces allow the generation of SOSL.

3. STIGMATIC OVOID LENSES

A SOSL is a lens composed of two Cartesian ovoid interfaces, which results in a rigorously stigmatic lens for only one pair of conjugated distances. As shown in Fig. 3, and considering all the defined distances given from the origin of coordinates $\mathcal{O}$, the parameters that describe a SOSL are the following: the distance of the point object $d_0 = \overline{\mathcal{O}P_0}$, the distance of the point image $d_2 = \overline{\mathcal{O}P_2}$, the distance of an intermediate point given by $d_1 = \overline{\mathcal{O}P_1}$, matching both the point image of the first surface and the point object of the second surface, the refractive index of the media before the first surface n_0, the refractive index of the lens n_1, the refractive index of the media after the second surface n_2, the axial position of the first sirface $\overline{\mathcal{O}V_0} = \zeta_0$, the axial position of the second surface $\overline{\mathcal{O}V_1} = \zeta_1$, and the vertex-surface distances given by ρ_a and ρ_b, for Σ_a and Σ_b surfaces, respectively. Using these parameters the axial thickness of the lens given by $t = \zeta_1 - \zeta_0$ is directly defined.

Under this formulation, the first surface passing through the point V_0 is considered, having as rigorous stigmatic points $\overline{V_0P_0} = d_0 - \zeta_0$ and $\overline{V_0P_1} = d_1 - \zeta_0$, and the second surface passing through point V_1 with stigmatic points $\overline{V_1P_1} = d_1 - \zeta_1$ and $\overline{V_1P_2} = d_2 - \zeta_1$. Hence, the surfaces composing the lens are in such a way that the rigorous stigmatism is preserved. Using this set of parameters it is possible to express the form parameters of both Cartesian surfaces in a single expression that can be used for any number of surfaces. Considering two surfaces Σ_k, where $k = 0, 1$, the index of refraction before each surface is $n_o = n_k$, the index of refraction after each surface is $n_i = n_{k+1}$, and the conjugated points are $z_o = d_k - \zeta_k$ and $z_i = d_{k+1} - \zeta_k$. Replacing these values in Eqs. (3)–(6), the following expressions are obtained:

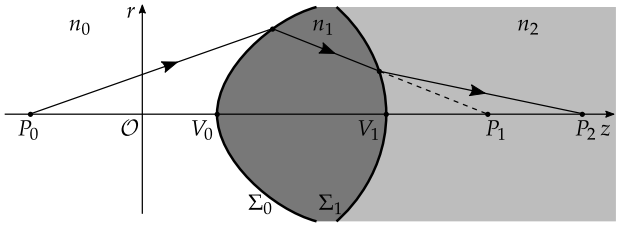

Fig. 3. Graphical scheme of a SOSL generated by the intersection of two Cartesian surfaces. The Cartesian surface Σ_0 is the surface able to form a perfect point image on P_1 from a point object on P_0. The surface Σ_1 is the surface able to form a perfect point image on P_2 from a point object on P_1 [33].

$$G_k = \frac{\left(\frac{n_{k+1}^2}{d_k-\zeta_k} - \frac{n_k^2}{d_{k+1}-\zeta_k}\right)^2}{n_k n_{k+1}\left(\frac{n_{k+1}}{d_{k+1}-\zeta_k} - \frac{n_k}{d_k-\zeta_k}\right)\left(\frac{n_{k+1}}{d_k-\zeta_k} - \frac{n_k}{d_{k+1}-\zeta_k}\right)}, \tag{14}$$

$$O_k = \frac{\frac{n_{k+1}}{(d_{k+1}-\zeta_k)} - \frac{n_k}{(d_k-\zeta_k)}}{(n_{k+1}-n_k)}, \tag{15}$$

$$T_k = \frac{\left(\frac{n_{k+1}+n_k}{(d_{k+1}-\zeta_k)(d_k-\zeta_k)}\right)^2 (n_{k+1}-n_k)}{4n_{k+1}n_k\left(\frac{n_{k+1}}{(d_k-\zeta_k)} - \frac{n_k}{(d_{k+1}-\zeta_k)}\right)}, \tag{16}$$

$$S_k = \frac{\frac{(n_{k+1}+n_k)}{(d_{k+1}-\zeta_k)(d_k-\zeta_k)}\left(\frac{n_{k+1}^2}{(d_k-\zeta_k)} - \frac{n_k^2}{(d_{k+1}-\zeta_k)}\right)}{2n_{k+1}n_k\left(\frac{n_{k+1}}{(d_k-\zeta_k)} - \frac{n_k}{(d_{k+1}-\zeta_k)}\right)}, \tag{17}$$

which according to the value of k define the form parameters of the respective surface Σ_0 or Σ_1.

A formulation for SOSL is derived using Eqs. (10) and (11) to replace Eqs. (14)–(17), obtaining the coordinates $z_k(\rho_k)$ and $r_k(\rho_k)$ of both surfaces Σ_k, with $k = 0, 1$. Because the conjugated points of both surfaces are measured relative to the vertex of each surface, the axial coordinate of the surfaces is displaced a distance ζ_k from the origin of coordinates $\mathcal{O}$. Hence, the intersection volume of the two Cartesian surfaces Σ_0 and Σ_1 shape a SOSL.

The Cartesian surfaces are formulated using ρ as a free parameter, defined as the distance between the vertex and any point on the surface. Given the range of values for parameter ρ, the values for the coordinates $z(\rho)$ and $r(\rho)$ that characterize both surfaces of the lens are obtained. These coordinates can be formulated also by a single parametric expression, given by

$$z_k(\rho_k) = \zeta_k + \frac{(O_k + T_k\rho_k^2)\rho_k^2}{1 + S_k\rho_k^2 + \sqrt{1 + (2S_k - O_k^2G_k)\rho_k^2}}, \tag{18}$$

$$r_k(\rho_k) = \pm\sqrt{\rho_k^2 - (z_k(\rho_k) - \zeta_k)^2}. \tag{19}$$

Because the rigorous stigmatism only occurs for a single pair of points, for an object point outside the stigmatic point, the system ceases to form a perfect point image and it is necessary to appeal to a paraxial regime, limiting the number of rays that access the system to form an aberrated image within approximate stigmatism conditions. In this paraxial regime or first-order theory, the optical systems can be characterized by its cardinal points, which are paraxial notions. So, for a rigorously stigmatic optical system, paraxial notions, in addition to being useless in this fourth-order theory, may also be meaningless because there is no limitation on the rays entering the system, whereas on the contrary for an object location d_0 and an image location d_2, the parameters d_1 and $t = \zeta_1 - \zeta_0$ allow characterizing the shape's parameters [Eqs. (14)–(17)] of a SOSL.

A Cartesian refractive surface is rigorously stigmatic only in a pair of points, for a specified refractive index, and this surface is unique, but it is important to say that a SOSL has infinite possibilities of shapes for this same pair of points. These different shapes are achieved by varying the parameters d_1 and

t, which adds degrees of freedom in the process of designing spherical aberration-free SOSL. It is worth mentioning that this formulation can be extended to consider an arbitrary number of Cartesian surfaces, and in the same way as the methodology proposed in Ref. [41], achieve a system free of spherical aberration.

4. ANALYTICAL RAY-TRACING METHOD

The formulation of an exact ray-tracing method, whereby we can verify the trajectory of a cone of rays when they go through an optical system, is essential in the area of optical design, which combined with optimization processes, is used to find the best configuration of a set of optical surfaces to perform as a high-quality optical system.

Figure 4 shows the trajectory $\overline{AI_0I_1B}$ followed by a ray through a singlet lens with refractive index n_1, immersed in a medium of refractive index n_0. This ray is refracted twice in points I_0 and I_1 on surfaces Σ_0 and Σ_1, respectively, to then reach point B. To develop a ray-tracing method through a SOSL, it is indispensable first to obtain the coordinates of the point I_0 and then the normal unit vector, necessary to calculate the unit vector of refracted ray using the Snell–Descartes law.

A. Interception Point between a Ray and a Cartesian Surface

To calculate the intersection point of a segment of the trajectory of the ray, the segment $\overline{AI_0}$, with the Cartesian surface Σ_0 (see Fig. 4), considering a Cartesian coordinates system where $r^2 = x^2 + y^2$, we define the source point A with coordinates (x_o, y_o, z_o), and point I_0 on surface Σ_0, with coordinates (x, y, z). If $\hat{u} = (u_x, u_y, u_z)$ is the unit vector indicating the direction from A to I_0, then the segment $\overline{AI_0}$ is expressed as the parametric equation

$$x = \frac{u_x}{u_z}(\lambda - z_o) + x_o, \tag{20}$$

$$y = \frac{u_x}{u_z}(\lambda - z_o) + x_o, \tag{21}$$

$$z = \lambda, \tag{22}$$

where λ is the parameter and $\rho^2 = x^2 + y^2 + z^2$ is written as

$$\rho^2 = \frac{z^2}{u_z^2} - 2z\left[\frac{u_x}{u_z}\left(\frac{u_x}{u_z}z_o - x_o\right) + \frac{u_y}{u_z}\left(\frac{u_y}{u_z}z_o - y_o\right)\right] + \left(\frac{u_x}{u_z}z_o - x_o\right)^2 + \left(\frac{u_y}{u_z}z_o - y_o\right)^2. \tag{23}$$

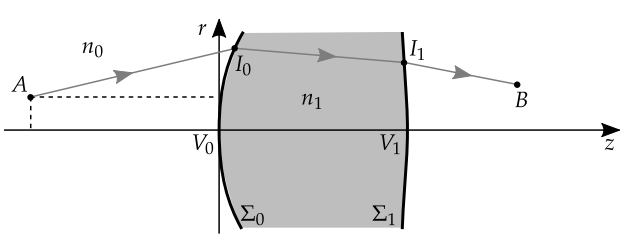

Fig. 4. Trajectory of a ray through a singlet lens.

To find an expression to get the z values where the segment $\overline{AI_0}$ intercepts the surface Σ_0, we first substitute Eq. (23) into Eq. (9). Getting rid of the radical by reordering and squaring onceresults in a quartic polynomial given by

$$Q_4 z^4 + Q_3 z^3 + Q_2 z^2 + Q_1 z + Q_0 = 0, \tag{24}$$

where Q_4, Q_3, Q_2, and Q_1 are constants given by

$$Q_4 = \frac{S^2}{u_z^4}, \tag{25}$$

$$Q_3 = -\frac{2S}{u_z^2}\left(GO - \frac{2S}{u_z}(b_x u_x + b_y u_y)\right), \tag{26}$$

$$Q_2 = GO\left(GO + \frac{O}{u_z^2} - \frac{4S}{u_z}(b_x u_x + b_y u_y)\right) + 2S^2(b_x^2 + b_y^2 + \frac{3}{u_z{}^2}(b_x u_x + b_y u_y)^2 + \frac{1}{u_z^2}(b_x u_y - b_y u_x)^2), \tag{27}$$

$$Q_1 = 2GO\left(\frac{O}{u_z}(b_x u_x + b_y u_y) - S(b_x^2 + b_y^2) - 1\right) + \frac{4S^2}{u_z}(b_x^2 + b_y^2)(b_x u_x + b_y u_y), \tag{28}$$

$$Q_0 = (b_x^2 + b_y^2)(GO^2 + S^2(b_x^2 + b_y^2)), \tag{29}$$

and

$$b_x = x_o - \frac{u_x}{u_z}z_o, \tag{30}$$

$$b_y = y_o - \frac{u_y}{u_z}z_o. \tag{31}$$

Equation (24) can be solved using an analytical method (e.g., Ferrari method) [42,43], resulting in the roots of this polynomial expression, consisting of four values of the z coordinate where the ray intersects with the Cartesian surface Σ_0. Replacing those values in Eqs. (20)–(22), we find the coordinates (x, y, z) of the point I_0, used to define the normal unit vector to the surface Σ_0 on this point.

1. Edge Thickness of SOSL

The edge thickness of these lenses can be calculated analytically. Considering the lines representing the ray in the previous section being parallel to the z axis, $u_x = u_y = 0$ and $u_z = 1$, we obtain from Eq. (24) a quartic polynomial given by

$$Q_{4k} z_k^4 + Q_{3k} z_k^3 + Q_{2k} z_k^2 + Q_{1k} z_k + Q_{0k} = 0, \tag{32}$$

with coefficients

$$Q_{4k} = S_k^2, \tag{33}$$

$$Q_{3k} = -2G_k S_k O_k, \tag{34}$$

$$Q_{2k} = G_k O_k^2 (G_k + 1) + 2 S_k^2 r_o^2, \tag{35}$$

$$Q_{1k} = -2 G_k O_k (1 + S_k r_o^2), \tag{36}$$

$$Q_{0k} = r_o^2 (G O_k^2 + S_k^2 r_o^2), \tag{37}$$

where $r_o^2 = x_o^2 + y_o^2$ and the subscript k indicates the surface composing the SOSL. Assuming that for the first surface the solution to Eq. (32) is given by $z_0 = a$ and for the second one a solution given by $z_1 = b$ is obtained, the edge thickness of the SOSL to the height r_o is then given by

$$t_e = b - a + t. \tag{38}$$

B. Application of Snell–Descartes Law to Cartesian Surfaces

The key component to formulate the Snell–Descartes law is the the normal unit vector, calculated according to the intersection point of a ray with a given direction of propagation and a Cartesian surface as shown above. Going back to the implicit expression of Cartesian surfaces [Eq. (7)], its derivatives with respect to x, y, and z are

$$\frac{\partial f}{\partial x} = -4 S x z + 4 T (x^2 + y^2 + z^2) x + 2 x O, \tag{39}$$

$$\frac{\partial f}{\partial y} = -4 S y z + 4 T (x^2 + y^2 + z^2) y + 2 y O, \tag{40}$$

$$\frac{\partial f}{\partial z} = -4 S z^2 + 4 T (x^2 + y^2 + z^2) z + 2 z O + 2 (G O z - S (x^2 + y^2 + z^2) - 1), \tag{41}$$

used to express the unit normal vector as

$$\hat{N} = \frac{\nabla f(x, y, z)}{|\nabla f(x, y, z)|} = \frac{\frac{\partial f}{\partial x}\hat{i} + \frac{\partial f}{\partial y}\hat{j} + \frac{\partial f}{\partial z}\hat{k}}{\sqrt{\left(\frac{\partial f}{\partial x}\right)^2 + \left(\frac{\partial f}{\partial y}\right)^2 + \left(\frac{\partial f}{\partial z}\right)^2}}. \tag{42}$$

Equation (42) determines the orientation of a normal vector to the Cartesian surface, which is outward when both conjugated points are real; also, when the point object is virtual, and the point image is real, in the rest of the cases, it is inward. This formulation is applicable without further consideration for cases where rays travel from left to right.

For a given incident unit vector, and by expressing the normal unit vector using Eq. (42), we implemented the Snell–Descartes law, which is used to find the refracted unit vector, expressed as

$$\hat{u}' = \eta \hat{u} - \left[\eta (\hat{N} \cdot \hat{u}) + \sqrt{1 - \eta^2 (1 - (\hat{N} \cdot \hat{u})^2)}\right] \hat{N}, \tag{43}$$

where η is the ratio between the previous refractive index and the posterior one to the surface, given by $\eta = n_o / n_i$. Given the unit incident vector $\hat{u}$, Eqs. (43) and (42) allow us to calculate the trajectory of a ray through a set of Cartesian surfaces, being the refracted unit vector of the current surface, the corresponding incident unit vector to the subsequent surface.

Using this ray-tracing formulation, we show, in the following section, some examples of the behavior of a bundle of rays through some SOSLs. This formulation allows us to trace rays that depart from the point object, going through the lens, to then form a perfect point image.

5. SIMULATED COMPUTATIONAL RESULTS OF SOSL

The Cartesian surfaces have generated a new interest associated with various modern applications and the current facilities for their production [2,9,13]. In this section, we show some designs of SOSL. We analyze how the variation in the entire range of values of the intermediate point d_1 and axial thickness t modify the values obtained by Eqs. (14)–(17) and thus obtain different shapes of SOSL.

Equation (15) formulates the curvature of the surfaces composing the singlet lens. The curvature of the first surface is obtained with $k = 0$, and for the second surface $k = 1$. In the following example, the vertex of the first surface matches with the origin of coordinates, so $\zeta_0 = 0$ and $t = \zeta_1$. While keeping the values of the indices of refraction fixed such that $n_2 = n_0$ and $n_1 > n_0$, the object distance d_0, image distance d_2, and axial thickness t are obtained from Eq. (15), with two equations for curvatures dependent on d_1. In Fig. 5 is shown the behavior of these curvatures, composing a SOSL where the paraxial curvatures of the first surface $O_0(d_1)$ and the paraxial curvature of the second surface $O_1(d_1)$ are identified by the solid and dashed lines, respectively. There we can deduce the SOSL shapes for a given range of values of the intermediate point d_1.

There are infinite possibilities of points object and image combinations, each of them resulting in a type or SOSL with a unique form or design. To classify all type of lenses, we define a dimensionless shape factor or bending, which is expressed as a function of the paraxial curvatures of both surfaces comprising the SOSL, written as

$$\sigma = \frac{O_0 + O_1}{O_0 - O_1} = -\frac{\left(\frac{n_1}{d_1 - t} - \frac{n_0}{d_2 - t}\right) + \left(\frac{n_1}{d_1} - \frac{n_0}{d_0}\right)}{\left(\frac{n_1}{d_1 - t} - \frac{n_0}{d_2 - t}\right) - \left(\frac{n_1}{d_1} - \frac{n_0}{d_0}\right)}. \tag{44}$$

This shape factor is analogous to the Coddington shape factor for bispherical lenses, used to minimize both spherical and coma aberrations [44].

As is shown in Appendix A, from Eq. (44) a quadratic equation with two solutions is obtained,

$$d_1 = \frac{-C_1 \pm \sqrt{C_1^2 - 4 C_2 C_0}}{2 C_2}, \tag{45}$$

where C_0, C_1, and C_2 are parameters given by Eqs. (A3)–(A5), which depend on σ. This relation between d_1 and σ makes it possible to link the shape factor with Eqs. (18) and (19).

In Fig. 6 are shown different shapes of rigorously stigmatic lenses according to the values of the shape factor σ, for cases where $n_1 > n_0 = n_2$. The shapes are grouped according whether the point object and point image are either real or virtual [34].

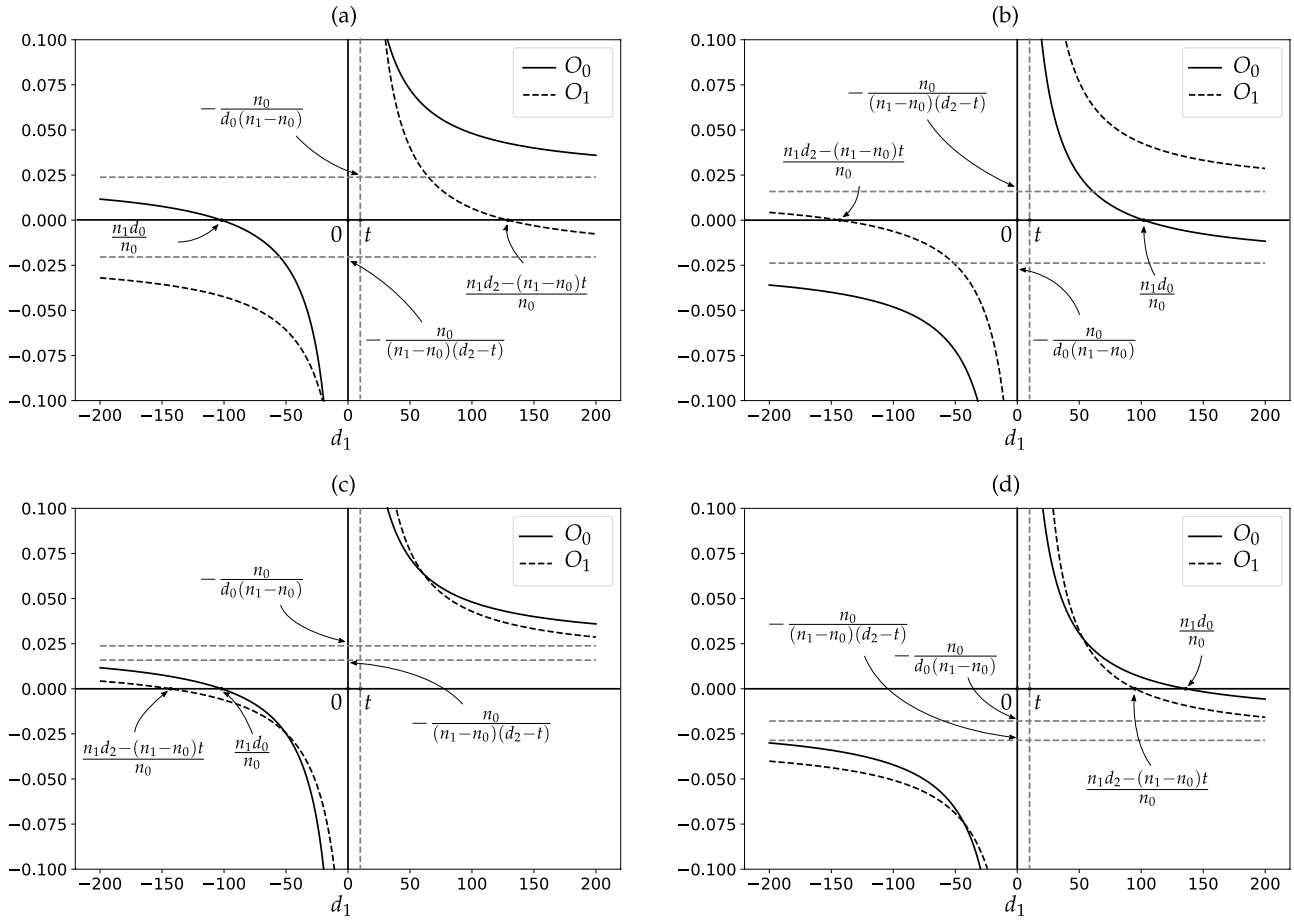

Fig. 5. Plot of the change of both paraxial curvatures O_0 and O_1 of the lens surfaces, while varying intermediate point d_1, regarding fixed values of $\zeta_0 = 0$, $\zeta_1 = 10$, $n_0 = n_2 = 1$, and $n_1 = 1.7$. (a) The point object and the point image are both real: $d_0 = -60$ and $d_2 = 80$. (b) The point object and the point image are both virtual: $d_0 = 60$ and $d_2 = -80$. (c) The point object is real and the point image is virtual: $d_0 = -60$ and $d_2 = 80$. (d) The point object is virtual and the point image is virtual: $d_0 = 80$ and $d_2 = 60$. The value of O_0 vanishes when $d_1 = n_1 d_0 n_0^{-1}$, and the value of O_1 does it when $d_1 = [n_1 d_2 - t(n_1 - n_0)]n_0^{-1}$. The vertical asymptotes are located at $d_1 = 0$ for the O_0 curve and at $d_1 = t$ for O_1 curve. The horizontal asymptote for the first surface is $O_0 = -n_0[d_0(n_1 - n_0)]^{-1}$ and for the second surface is $O_1 = n_0[(n_1 - n_0)(t - d_2)]^{-1}$.

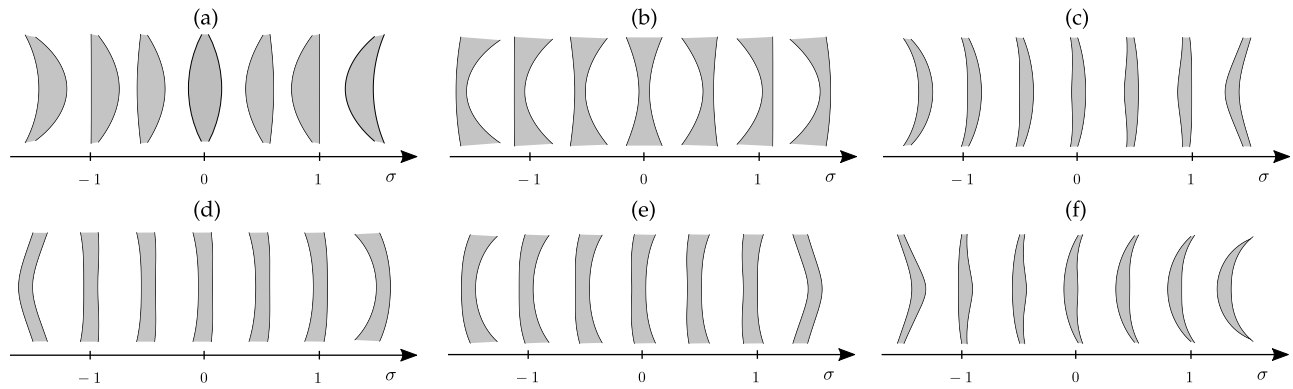

Fig. 6. Different simulated shapes of SOSL according to the form parameter σ. (a) Variations of the lens shape for both real rigorously stigmatic points. (b) Lens shape for both virtual rigorously stigmatic points. (c) Lens shape for a real point object and virtual point image where $|d_0| < |d_2|$. (d) Lens shape for a real point object and virtual point image where $|d_0| > |d_2|$. (e) Lens shape for a virtual point object and real point image where $|d_0| < |d_2|$. (f) Lens shape for a virtual point object and real point image where $|d_0| > |d_2|$. All cases are obtained maintaining fixed values of the index of refraction such that $n_1 > n_0 = n_2$.

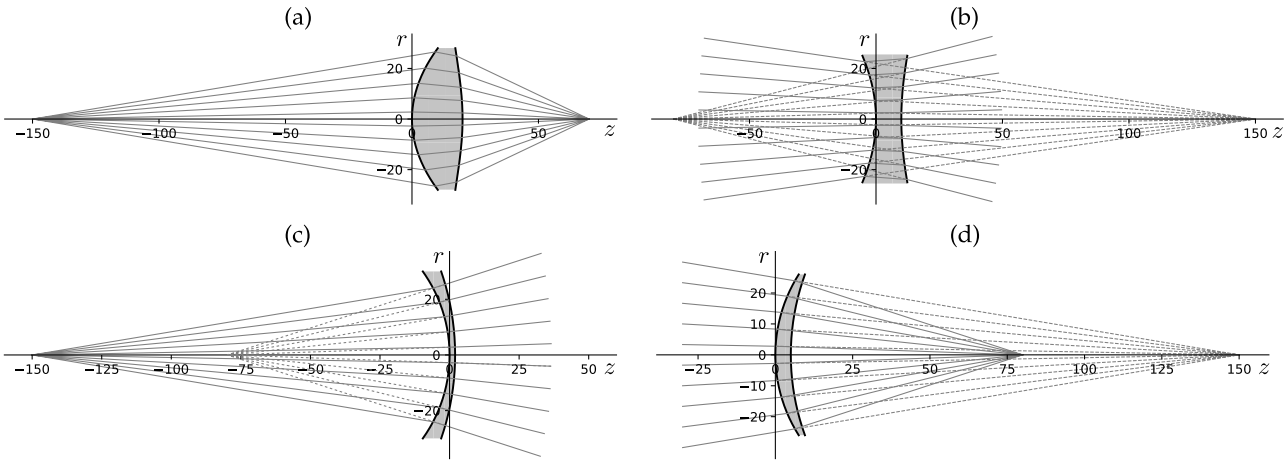

Fig. 7. Some computational simulations of SOSL using refractive indices $n_0 = n_2 = 1.0$ and $n_1 = 1.7$, and the vertex of the first surface located at $\zeta_0 = 0$. (a) Real point image from a real point object with $d_0 = -150$, $d_2 = 70$, $\sigma = 0.444$, $t = \zeta_1 = 20$, and $t_e = 6.934633308802912$ for a value of $r = 28$. (b) Virtual point image from a virtual point object with $d_0 = 150$, $d_2 = -70$, $\sigma = 0.360$, $t = \zeta_1 = 10$, and $t_e = 17.74174828953162$ for a value of $r = 25$. (c) Virtual point image from a real point object with $d_0 = -150$, $d_2 = -80$, $\sigma = 3.524$, $t = \zeta_1 = 2$, and $t_e = 6.604481025026159$ for a value of $r = 30$. (d) Real point image from a virtual point object with $d_0 = 150$, $d_1 = 80$, $\sigma = 4.485$, $t = \zeta_1 = 5$, and $t_e = 2.0166059914527708$ for a value of $r = 26$.

If both rigorously stigmatic points are real, the lenses obtained are positive meniscus and biconvex as shown in Fig. 6(a). If both rigorously stigmatic points are virtual, the lenses obtained are negative meniscus and biconcave as shown in Fig. 6(b). When the point object is real but the point image is virtual, the shapes obtained are shown in Figs. 6(c) and 6(d), depending on whether $|d_0| > |d_2 - t|$ or otherwise. This condition is also held for the opposite combination of rigorously stigmatic points. If point object is virtual and point image is real, the resulting forms are shown in Figs. 6(e) and 6(f), that, because of the reciprocity principle, are the same shapes obtained in the previous configuration but vertically flipped.

In Fig. 7 are shown some computational results with different configurations of the point object and the point image, related to different values of shape factor σ and hence different SOSL designs. The resulting SOSLs are corroborated using our ray-tracing method. In the same way that bi-aspherical lenses are thin, these ovoid lenses can produce thin lenses with large aperture as is shown in Fig. 7(c).

The developed formulation also contains solutions for point object and point image at the infinite as shown in Fig. 8(a). A SOSL design with the point object at the infinite is composed by one conic surface (first surface) and a quartic surface (second surface), and it has the focus located at the image position. The same results from imaging a finite point object at the infinite, but instead of the first surface, the second surface is a conic. In Fig. 8(b) is shown another special case, an afocal system, that is able to form a perfect point image at infinity from a point object at infinity. Commonly, an afocal system is composed of two spherical singlet lenses, but using this formulation is obtained using a SOSL composed of two conic surfaces. Using this formulation a series of SOSLs is derived, and as a summary, in Table 2, were included some designs for the case where $n_1 > n_0 = n_2$ and $|d_0| > |d_2 - t|$.

Furthermore, it is evident that in SOSL lenses there is a reduction of the meridional coma for certain value of σ as is shown in

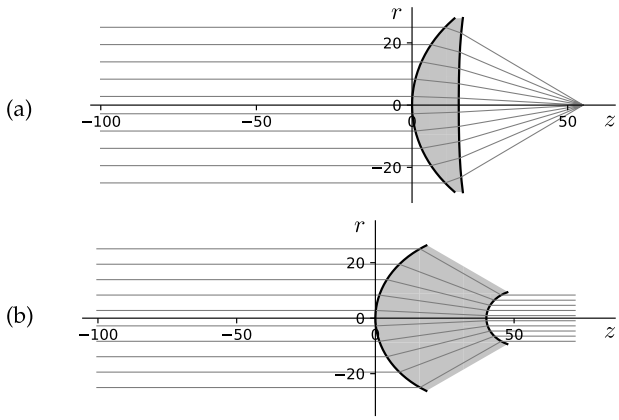

Fig. 8. SOSL designs using refractive indices $n_0 = n_2 = 1.0$ and $n_1 = 1.7$. (a) Object at infinity with $d_2 = 55$, $\sigma = 1.114$, and $t = \zeta_1 = 15$. (b) Both object and image at infinity, with $\sigma = -2.0$ and $t = \zeta_1 = 40$.

Fig. 9. In the area of optical design, the elimination of the reduction of aberrations that prevent the correct formation of the image is important. Using these type of lenses, we can achieve several lenses with zero spherical aberration and a minimum amount of meridional coma. As we can appreciate in Fig. 10, there are other types of aberrations presented in this types of lenses. In this figure we show some spot diagrams for different image planes for an image produced by the off-axis point object in Fig. 9, where the presence of astigmatism is clearly noticed.

There are several applications of aspherical surfaces in the area of the optical design; one of them is the reduction of the number of spherical surfaces along with the compensation of aberrations to a determined order. In addition to aspherical surfaces, we believe that the proposed SOSLs, or even better, a set of Cartesian surfaces, could be used to design optical imaging

Table 2. SOSL Shape for a Real Object and Real Image, $d_0 < 0$ and $d_2 - t > 0$, According to the Range of Values of Intermediate Point d_1, Regarding $n_1 > n_0 = n_2$ and $|d_0| < |d_2 - t|$

	Shape Factor (σ)			
Lens Type	$d_0 < 0$ and $d_2 > t$	$d_0 > 0$ and $d_2 < t$	$d_0 < 0$ and $d_2 < t$	$d_0 > 0$ and $d_2 > t$
Biconvex	$-1 < \sigma < 1$	—	$-1 < \sigma < 1$	—
Biconcave	—	$-1 < \sigma < 1$	—	$-1 < \sigma < 1$
Plane-convex	$\sigma = -1$	—	—	—
Convex-plane	$\sigma = 1$	—	—	—
Plane-concave	—	$\sigma = -1$	—	—
Concave-plane	—	$\sigma = 1$	—	—
Convex-concave	$\sigma > 1$	$\sigma > 1$	$\sigma > 1$	$\sigma < -1$
Concave-convex	$\sigma < -1$	$\sigma < -1$	$\sigma < -1$	$\sigma > 1$

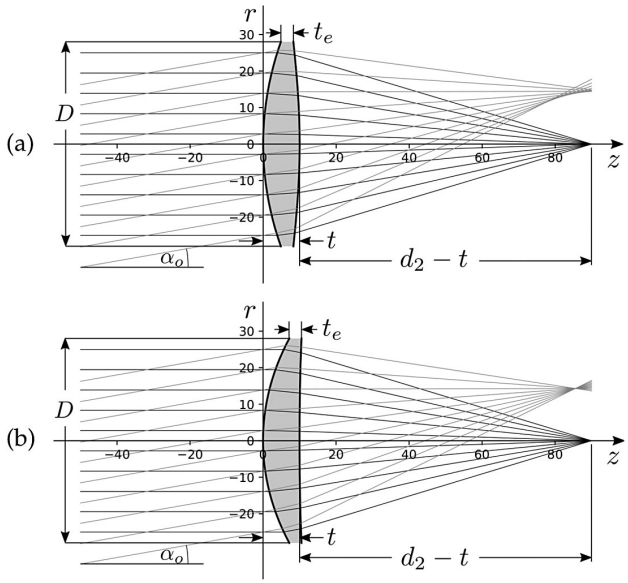

Fig. 9. Reduction of off-axis aberrations on the meridional plane in SOSLs for point objects at infinity. In both images the common parameters are the indices of refraction $n_0 = n_2 = 1$ and $n_1 = 1.7$, the conjugated points $d_0 = -\infty$ and $d_2 = 90$ (mm), the axial thickness of the lens $t = \zeta_1 = 10$ (mm), the degree of inclination $\alpha_o = 10°$ of a fan of rays coming from an off-axis point object located at infinity, and the diameter of the lens given by $D = 56$ (mm). (a) A SOSL design with edge thickness $t_e = 3.4234459735169027$ (mm) showing a considerable amount of off-axis aberrations for a shape factor $\sigma = 0.4104803493449782$. (b) A SOSL design with edge thickness $t_e = 3.3429500425595355$ (mm) showing a reduction of aberrations in the image for the same off-axis point object for a shape factor $\sigma = 1.13633512735255$.

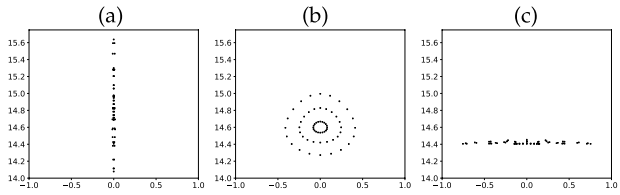

Fig. 10. Spot diagrams of different image planes along the z axis for the image resulting from the off-axis point object in Fig. 9. While varying the image plane position, different sport diagrams are obtained, shown in (a), (b), and (c), where the presence of astigmatism is evident. The position of image plane in (a) is $z = 87.9$ (mm), in (b) is $z = 86.6$ (mm), and in (c) is $z = 85.5$ (mm).

systems just like eyepieces for telescopes, microscopes objectives, and telecentric lenses, where the latter are used in machine vision and optical lithography. From the designs presented in patents [9–12], we see that some of the surfaces used to design the proposed optical system are aspherical surfaces formulated using the standard aspherical equation, which makes use of a set of coefficients. Those aspherical surfaces are used to compensate for spherical aberration according to the order of the coefficients, simplifying the size, weight, and design of the system. Our closed-form formulation could be extended to a set of Cartesian surfaces, that have varying the degrees of freedom given by the form parameters, to propose the design of this type of optical imaging system.

6. CONCLUSIONS

We have obtained a parametric formulation for Cartesian ovals given by Eqs. (10) and (11) along with the form parameters from Eqs. (3)–(6), which has as a particular case the Schwarzschild formula for conics. Using this formulation, a new formulation is obtained to design ovoid singlet lenses given by Eqs. (18) and (19), where the form parameters, expressed in Eqs. (14)–(17), offer a degree of freedom allowing us to obtain infinite solutions for these types of lenses. This formulation has the advantage of being capable of being extended to an arbitrary number of surfaces and being able to handle both refractive and reflective surfaces, for objects or images either real or virtual. It is important to highlight that this parametric expression for Cartesian ovals can be considered a closed-form expression of aspherical optical surfaces. These results constitute the basic elements for the spherical aberration-free imaging systems, by designing SOSLs such as biconvex, biconcave, and meniscus singlet lenses, using a range of values for the shape factor σ given by Eq. (44) as shown in Table 2. This shape factor can be seen as a generalized Coddington shape factor used to minimize spherical aberration in bispherical lenses. Considering this shape factor as a degree of freedom, we believe that it can be an important element for the adaptation of these systems to the study of the conditions under which an the aplanatism condition can be adapted for off-axis objects. Additionally, we implemented an analytical ray-tracing method based on the vector Snell–Descartes law.

This method allowed us to carry out the ray tracing through SOSL for on-axis and off-axis point objects, corroborating the perfect point imaging for the on-axis case.

We believe that this outstanding formulation can contribute to the optical design area, with different applications in many areas such as microscopy and astronomy. Equations (18) and (19) are parametric equations representing all types of Cartesian surfaces that allow us to calculate any cloud of points describing both surfaces of the lens. The number of points can be any number of data and is independent for each surface, allowing the definition of an error function and the use of this data by computer-aided design software, resulting in SOSL designs, which can be used by computer-aided manufacturing software.

APPENDIX A: THE LINK BETWEEN SHAPE FACTOR AND SOSL FORMULATION

To express SOSL formulation [Eqs. (18) and (19)] as a function of shape factor σ, it is necessary to write the d_1 parameter as a function of σ. From Eq. (44) it is possible to reorder terms and obtain a second-order polynomial in d_1 given by

$$C_2 d_1^2 + C_1 d_1 + C_0 = 0, \tag{A1}$$

which results in two solutions,

$$d_1 = \frac{-C_1 \pm \sqrt{C_1^2 - 4C_2C_0}}{2C_2}, \tag{A2}$$

where

$$C_2 = n_0\,(n_1 - n_0)\left[\frac{(\sigma-1)}{d_0} - \frac{(\sigma+1)}{d_2 - t}\right], \tag{A3}$$

$$C_1 = n_0\,(\sigma-1)\left(\frac{d_2 n_1}{d_2 - t} - \frac{t\,(n_1 - n_0)}{d_0}\right) + [2n_1 - n_0\,(\sigma+1)]\left(\frac{n_0 t}{d_2 - t} + n_1\right), \tag{A4}$$

$$C_0 = n_1 t\,(\sigma-1)\,(n_1 - n_0)\,. \tag{A5}$$

The negative sign in Eq. (A2) corresponds to values of d_1 inside of the lens; otherwise, it is positive. Equation (A2), along with Eqs. (A3)–(A5), allows us to express d_1 as a function of σ and hence link the shape factor with Eqs. (18) and (19).

Acknowledgment. The authors are grateful for the financial support from the Departamento Administrativo de Ciencia, Tecnología e Innovación de Colombia, and from the Vicerrectoría de Investigación y Extensión of the Universidad Industrial de Santander.

Disclosures. The authors declare no conflicts of interest.

REFERENCES

1. R. E. Fischer, B. Tadic-Galeb, P. R. Yoder, R. Galeb, B. C. Kress, S. C. McClain, T. Baur, R. Plympton, B. Wiederhold, and A. J. Grant, *Optical System Design*, 2nd ed. (McGraw-Hill, 2008), Vol. **1**.
2. M. B. Villarino, "Decartes' perfect lens," arXiv preprint arXiv:0704.1059 (2007).
3. R. Güther, "Descartes ovaloides for negative refractive indices and their aplanatic cases," Optik **119**, 577–583 (2008).
4. C.-C. Hsueh, T. Elazhary, M. Nakano, and J. Sasian, "Closed-form sag solutions for Cartesian oval surfaces," J. Opt. **40**, 168–175 (2011).
5. J. C. V. Estrada, Á. H. B. Calle, and D. M. Hernández, "Explicit representations of all refractive optical interfaces without spherical aberration," J. Opt. Soc. Am. A **30**, 1814–1824 (2013).
6. R. Descartes, *Discours de la méthode pour bien conduire sa raison et chercher la vérité dans les sciences, with three appendices: La Dioptrique* (1637).
7. C. Huygens, *Traité de la lumière:...* (Chez Pierre vander Aa, marchand libraire, 1920).
8. H. Gross, H. Zügge, P. Martin, and F. Blechinger, *Handbook of Optical Systems: Aberration Theory and Correction of Optical Systems* (Wiley, 2007), Vol. **3**.
9. K. Sato, "Single focus lens," U.S. patent 6,930,841 (August 16, 2005).
10. C.-C. Liao, "Compact lens system," U.S. patent 7,236,314 (June 26, 2007).
11. C.-C. Liao, "Micro lens," U.S. patent 7,477,459 (January 13, 2009).
12. Y. J. Jo and J. H. Baik, "Optical system," U.S. patent 10,444,470 (October 15, 2019).
13. J. P. Sutter and L. Alianelli, "Ideal Cartesian oval lens shape for refocusing an already convergent beam," AIP Conf. Proc. **2054**, 030007 (2019).
14. D. Michaelis, P. Schreiber, and A. Bräuer, "Cartesian oval representation of freeform optics in illumination systems," Opt. Lett. **36**, 918–920 (2011).
15. J. C. Valencia-Estrada and J. Garca-Márquez, "On-axis diffraction-limited design of bi-parabolic singlet lenses," Optik **193**, 162970 (2019).
16. D. McCloskey and J. Donegan, "Planar elliptical solid immersion lens based on a Cartesian oval," Appl. Phys. Lett. **103**, 091101 (2013).
17. H. C. King, *The History of the Telescope* (Courier, 2003).
18. E. Abbe, "Beiträge zur theorie des mikroskops und der mikroskopischen wahrnehmung," Arch. Mikrosk. Anat. **9**, 413–418 (1873).
19. D. Lynden-Bell, "Exact optics: a unification of optical telescope design," Mon. Not. R. Astron. Soc. **334**, 787–796 (2002).
20. R. Willstrop and D. Lynden-Bell, "Exact optics–II. exploration of designs on-and off-axis," Mon. Not. R. Astron. Soc. **342**, 33–49 (2003).
21. H. Mashaal, D. Feuermann, and J. M. Gordon, "Basic categories of dual-contour reflective-refractive aplanats," Opt. Lett. **40**, 4907–4910 (2015).
22. H. Mashaal, D. Feuermann, and J. M. Gordon, "Expansive scope of aplanatic concentrators and collimators," Appl. Opt. **58**, F14–F20 (2019).
23. G. Wassermann and E. Wolf, "On the theory of aplanatic aspheric systems," Proc. Phys. Soc. B **62**, 2–8 (1949).
24. E. M. Vaskas, "Note on the Wasserman-Wolf method for designing aspheric surfaces," J. Opt. Soc. Am. **47**, 669–670 (1957).
25. B. Jurek, "Systèmes rigoureusement aplanétiques à deux surfaces," Optica **6**, 222–233 (1959).
26. W. Welford, "Vi aplanatism and isoplanatism," in *Progress in Optics* (Elsevier, 1976), Vol. **13**, pp. 267–292.
27. M. Born and E. Wolf, *Principles of Optics: Electromagnetic Theory of Propagation, Interference and Diffraction of Light* (Elsevier, 2013).
28. M. Krautter, "Aplanatic two-surface systems: the optics of our grandfathers," in *Optical System Design, Analysis, Production for Advanced Technology Systems* (International Society for Optics and Photonics, 1986), Vol. **655**, pp. 127–137.
29. J. C. Valencia-Estrada, R. B. Flores-Hernández, and D. Malacara-Hernández, "Singlet lenses free of all orders of spherical aberration," Proc. R. Soc. A **471**, 20140608 (2015).
30. R. G. González-Acuña and H. A. Chaparro-Romo, "General formula for bi-aspheric singlet lens design free of spherical aberration," Appl. Opt. **57**, 9341–9345 (2018).
31. R. G. González-Acuña, H. A. Chaparro-Romo, and J. C. Gutiérrez-Vega, "General formula to design a freeform singlet free of spherical aberration and astigmatism," Appl. Opt. **58**, 1010–1015 (2019).

32. J. C. Valencia-Estrada and J. Garca-Márquez, "Freeform geometrical optics I: principles," Appl. Opt. **58**, 9455–9464 (2019).
33. J. C. Valencia-Estrada and H. Bedoya-Calle, "Lentes asféricas ovales," Mexican patent application MX/a/2012/010025 (August 30, 2012).
34. A. Silva-Lora and R. Torres, "Explicit Cartesian oval as a superconic surface for stigmatic imaging optical systems with real or virtual source or image," Proc. R. Soc. A **476**, 20190894 (2020).
35. K. Schwarzschild, "Untersuchungen zur geometrischen optic II," Astron. Mitt. Kniglichen Sternwarte Göttingen **10**, 4–28 (1905).
36. A. Greynolds, "Superconic and subconic surface descriptions in optical design," in *International Optical Design Conference* (Optical Society of America, 2002), paper IMA1.
37. J. P. Southall, "Aplanatic (or Cartesian) optical surfaces," J. Franklin Inst. **193**, 609–626 (1922).
38. J. C. V. Estrada, "Manufactura CNC de superficies ópticas correctoras," Ph.D. thesis (Centro de Investigaciones en Optica, A.C., 2015).
39. S. Cho, "Explicit superconic curves," J. Opt. Soc. Am. A **33**, 1822–1830 (2016).
40. D. Reshidko, "Topics in modern lens design," Ph.D. thesis (College of Optical Sciences, 2016).
41. R. G. González-Acuña and J. C. Gutiérrez-Vega, "General formula to eliminate spherical aberration produced by an arbitrary number of lenses," Opt. Eng. **58**, 085106 (2019).
42. H. Turnbull, *Theory of Equations (University Mathematical Texts)* (Oliver and Boyd, 1957). Method invented by Lodovico Ferrari at the request of Cardano Hieronymus and published in 1545, in his Artis Magnae, Sive de Regulis Algebraicis, liber unus.
43. S. L. Shmakov, "A universal method of solving quartic equations," Int. J. Pure Appl. Math. **71**, 251–259 (2011).
44. T. T. Smith, "Spherical aberration in thin lenses," Phys. Rev. **19**, 276–277 (1922).